Pedestrian flow in two dimensions: Optimal psychological stress leads to less evacuation time and decongestion

M. Ramírez, B. A. Toledo, F. Torres, J. Rogan, J. A. Valdivia, and P. Correa-Burrows

Pedestrian Flow in 2D: Optimal psychological stress leads to less evacuation time and decongestion

M. Ramírez, B. A. Toledo, F. Torres, J. Rogan, and J. A. Valdivia

Departamento de Física, Facultad de Ciencias,

Universidad de Chile, Casilla 653, Santiago, Chile 7800024 and

Centro para el Desarrollo de la Nanociencia y la Nanotecnología (CEDENNA),

Avda. Ecuador 3493, Santiago, Chile 9170124

P. Correa-Burrows

Instituto de Nutrición y Tecnología de los Alimentos,

Universidad de Chile, El Líbano 5524, Santiago, Chile 7830490

(Dated: July 27, 2021)

Abstract

Collective motion is an innate ability of all living systems, which depends on physiological and psychosocial factors in the case of humans. Such a collective organization is becoming of great interest in collective motion in human crowds. Using a cellular automaton (CA) simulation model, we demonstrate that emergency egress from a two-dimensional corridor with optimal stress leads to less evacuation time and efficient mass evacuations. We study how three types of stress (i.e., mild stress, optimal stress and anxiety) described in the literature have a significant impact on the collective dynamics. We found that low-stress levels could decrease the evacuation time in an entire occupied room since agents choose alternative routes rather than the shortest path to the exit and display cooperative behavior. Therefore, the combination of mild and optimal stress can lead to efficient evacuations. Also, CA simulations may be used to find safer and more efficient ways to conduct mass evacuation procedures.

I. INTRODUCTION

Collective motion is a common phenomenon that emerges in systems that involve living entities, from large to microscopic [1–6]. Regardless of size, it depends on a combination of external (*e.g.* exposure to a potentially threatening event) and internal drivers (*e.g.,* the response to stressful stimuli). Such a collective organization is an adaptive regulatory mechanism that allows better survival probability, better access to information and resources, and better decision-making abilities [7, 8]. Although Biology plays a major role in the collective movement of organisms, these dynamics can be easily understood due to local and non-local interactions of particles [9]. Thus, they have been widely studied in fields as diverse as the Physics of plasmas, fluids, and solids [10–13]. For example, the movement of a group of animals, such as fish or birds [1, 2], can sometimes resemble the complex behavior displayed by water going through a nozzle. Similar dynamics can be found in humans [3–6], with psychological elements [14–16]. For example, Fig. 1(a) shows the complex motion of a crowded situation at a massive social event (*e.g.,* a music concert), where obstacles are also present. Similarly, Fig. 1(b) displays the dynamic of a herd of sheep changing corrals. In these systems, the complex collective behavior results from the combination of individual abilities of the constituent blocks or agents and the social, cultural, and psychological aspects of their
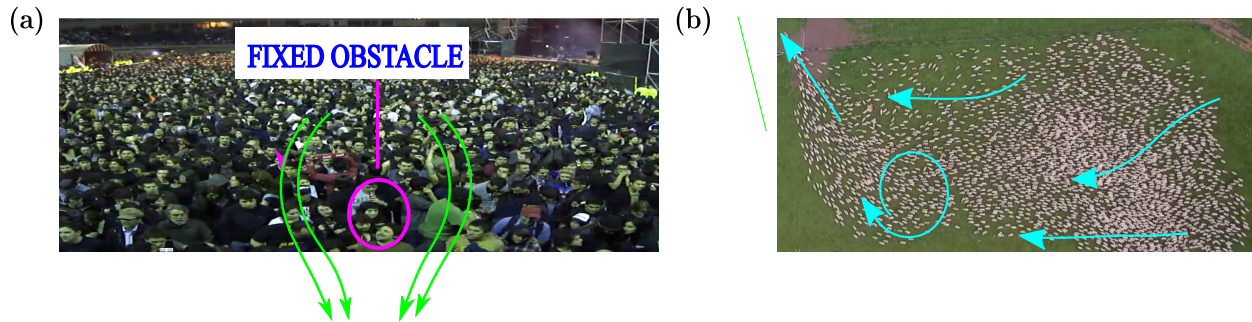
2

interaction with neighboring individuals.

FIG. 1. (color online) Different situations of massive flows of agents: (a) Screenshot of a massive evacuation after a music concert. If an obstacle exists, like in the screenshot, the movement of the rest of the agents can become complex (*i.e.* not laminar) which can increase the overall level of anxiety of the agents. (b) Movement of a herd of sheep changing corrals. We mark some particular agents' future movements to display some of the complex behavior that can appear. All these pictures were taken from videos available in [17, 18].

Scientific research on the collective motion of organisms has dramatically benefited from the contribution of physicists, computer scientists, and engineers, who have explored the mechanistic basis of this phenomenon [19]. Depending on the researcher's area of specialty, there are mainly two ways to study this problem: one is to observe from the field of psychology how a group of people behaves and try to draw conclusions. The other approach, which we will implement in this publication, is to consider the essential elements of human behavior to obtain conclusions from the macroscopic movements of a group of people. Beyond questions such as why collective movement occurs and its ultimate function, interest remains high in studying the 'how' of the movement because of its implications for mass emergency planning and management [20–23]. Events triggering a mass evacuation procedure may include fires in crowded buildings, sports stadium crushes, air or train crashes, sinking ships, terrorist attacks of any kind, and natural disasters. Similarly, amid the COVID-19 pandemic, the 'how' of the movement becomes of utmost relevance. While countries try very hard to return to some normality; efforts are still needed to keep social-distancing discipline. Pedestrian dynamics might help determine some of the constraints imposed to create the conditions for a safer transition back to normality.

Among others, individual-based models have used stochastic differential equations [24],

difference equations [25–27], and cellular automaton (CA) [28, 29]. In previous work, we used the approach by Varas *et al.* to study the fundamental features of crowd dynamics. Our analysis's major contribution is the inclusion of psychological effects, as they can produce non-trivial collective phenomena in the resulting dynamics [29]. We did so by relying on the model by social psychologists Robert Yerkes and John D. Dodson, an empirical model of stress and performance, proposed in the early 20th century [30], and subsequently validated by neuroimaging and neuroendocrine studies on stress physiology [31, 32]. Also known as the Yerkes-Dodson Law (YDL), the model posits a marginally decreasing relationship between stress and individual performance, which is well-represented by an inverted-U shape, as shown in Figure 2. According to the YDL, elevated stress levels –represented in Fig. 2 as a comfort zone leading to optimal activity levels– can actually improve the individual performance. Increasing arousal helps to focus motivation and attention on a particular task (*e.g.*, recognize cues or alarms, arrive at the exit, and identify that others obstruct it to mention a few), but only up to a certain threshold. When stress becomes excessive and reaches the point of anxiety or distress, performance starts to diminish, and too much anxiety can impair someone's ability to concentrate and choose the most efficient course of action. At this point, performance is no longer optimal, while panic and ineffectiveness become common responses. It follows that the individual behavior must have obvious consequences for the collective motion during emergencies, where different agents express different stress levels. How evacuees deal with stress in an emergency procedure is key to successfully conducting the process in terms of egress time, safety, and even the number of victims. Specific components of the evacuation time, such as the distribution of recognition time and response time are highly determined by the individual's skills to manage stress [33].

Despite major advances in computer-based simulations and data processing, experiments in virtual environments of crowd dynamics have failed to account for some essential psychosocial driving parameters in the collective behavior [33, 35, 36]. As Moussaïd *et al.* admit, several case studies of specific emergency evacuations have revealed patterns of emergency exiting that were not predicted by simulations based on analogies of particle and animal dynamics [37]. A deep understanding of moving crowds' basic and robust behavior is pivotal to develop effectively evacuation strategies [38], where the role of stress and social interactions are included in the dynamics. Here, CA simulations in a two-dimensional corridor model are used to examine egress behavior, and how the three types of stress (i.e., mild stress,
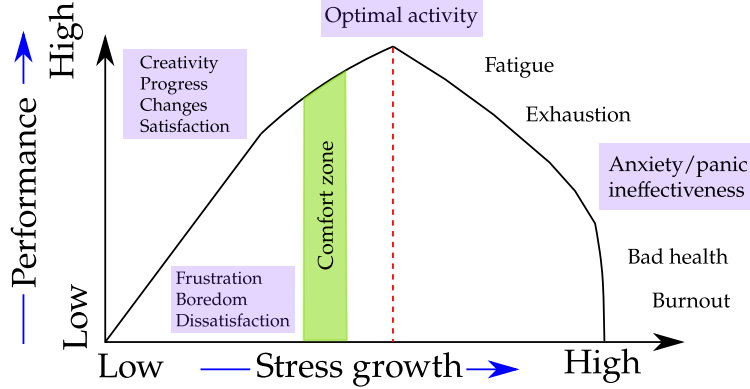
FIG. 2. (color online) Schematic diagram of performance as a function of stress, showing two general types of responses to stress, one before the optimal range of decisions, and another after this point. Source: This model was taken from the works by [30, 34].

optimal stress and anxiety), previously distinguished in the literature for individuals affect the management and efficiency of the evacuation process. This model naturally introduces a quantitative analysis of the types of stress through the randomness level of individual agents' movements. Numerical simulations display different evacuation behaviors independently of the specific numerical value of the stress. We hypothesize that both mild stress and anxiety result in a person's exiting response being ineffective, which compromises the evacuation efficiency. However, optimal stress, or stress that is manageable leads to less collective evacuation time and congestion at the exit. At any given time, we will have an evolving distribution of agents' stress that will affect in a non-trivial manner the collective behavior of the exit dynamics. In addition, it is important to realize that it is not obvious how to obtain real data, what to measure, and under what control conditions. The overall behavior of one individual, a family or a big crowd may end up being quite different, and there is a need to separate the individual behavioral complexities from the emergent collective dynamics. For example, the response of individuals may differ when participating in an emergency training exercise and an equivalent real stressful situation. One possibility is to use simulations to try to ascertain what are the relevant variables that we should try to measure and pursue, how effective parametrizations could be tested, and how comparison with different simulations could eventually be made. We should remember that at the end, we would like to have simulations that are able to parametrize in an effective manner, the individual's behavior, and collective interactions so that they can be applied in different

contexts such as the design of building and school, evacuation of events, public transport, how to guarantee social distance in open and close spaces, among others. Hence, this is the road we are taking in this manuscript.

We organize the paper as follows: In the next section, we introduce our model and describe the methodology for implementing it while analytically deriving expressions for simple scenarios that will guide the discussion. Afterward, we present the results. The manuscript is closed with a summary, where we draw the main conclusions and project future instances for our work.

II. METHODS

We model the agents' dynamic with CA simulations. A detailed review can be found in Ref. [39]. CA are mathematical idealizations of physical systems in which space and time are discrete and physical quantities take on a finite set of discrete values. This proposal intends to use the CA originally put forward by Von Neumann in 1963 [40] and applied to different idealizations of the physical reality, such as traffic problems [41–44], large-scale pedestrian movements [45], fluvial evolution [46], growth interface in solids [47], or facial recognition [48], among many others. The approach can represent physical systems to the point that is successfully used today in the German state of North-Rhine Westphalia [49].

In our simulations, the discrete variables will be the time step, the agents' position, and decisions taken by each of them in a given time step. Here, for simplicity, we will consider a fixed room of size $L_x \times L_y$ discretized into unit cells that are either empty or occupied by only one agent. According to closeness to the door, a single floor field (FF) strength has been assigned to each cell using the strategy suggested in Ref. [28]. Lower values correspond to cells closer to the exit, and thus this static FF indicates to the pedestrian the way to the exit. We allow movements in the diagonal, vertical, and horizontal directions along the grid, producing non-trivial dynamics that do not typically occur when restricting the movement only in the horizontal and vertical directions. The relative cost of moving to a diagonal nearest neighbor cell instead of moving to a vertical or horizontal nearest neighbor cell is $\lambda = 1.5$. We chose this specific value of λ to make comparisons with previous results, simplify the visualization of the floor field, and preserve the original spirit of the CA, which is to make coarse grain parametrizations, and from there, obtain results that could be compared

with experiments. In any case, we performed the same calculations for three different values of λ (1.25, $\sqrt{2}$, 1.5). The results do not vary much when λ varies around the $\sqrt{2}$ value. Finally, more than representing an exact Euclidean distance, in this CA model, the value of λ is related to the relative importance of the motion along the grid or to the diagonals (is a parametrization of the agents' interaction). What is relevant (at least for values close to $\lambda = \sqrt{2}$) is not only to be able to move along the diagonal. Also, that the interaction is beyond the nearest neighbors'.

As we introduce stress into the dynamics, the movement choices will change according to the agent's stress level. All agents can choose only one of their eight nearest cells to move. Inspired by our recent model [29], we define three possible movement intentions, depending on the stress level. Under mild stress, the agent searches for the lowest value of floor field among the eight neighboring cells. If the cell is empty, it tries to move to that cell. Under optimal stress, the agent looks, among the eight nearest neighbors, for the cells with a lower value than its own. If one of these cells is free, the agent tries to move to the one with the lowest available value. Last, under anxiety, the agent searches all eight neighboring cells, regardless of their value. Then it randomly chooses one of the empty cells and tries to move to it, regardless of the floor field value. If the agent finally moves to the chosen cell in this time step, its stress is reduced by one; otherwise, its stress increases. These definitions of possible movements complicate the available possibilities that agents have and, in high-density situations, compact the occupation of agents around the door by having more places to move. The model resembles an inverse U-shaped relation between arousal and performance, observed in both human and animal models [50–52], and denoting a high resemblance to the Yerkes–Dodson curve [31].

This implementation of the movement allows not only along the horizontal and vertical directions, but also along the diagonals, give rise to new two-dimensional evacuation dynamics. The agents are allowed to use only one cell at a given time, and our program will move all agents in the room until they have all left the room. Then, the program measures the number of steps it takes for a group of agents to act above. On an average of 1000 simulations, we will call this the elapsed simulation time $\langle T \rangle$. The rules of movement are not trivial to obtain since they must show the observed path followed by the agents in a precise way. It is expected that the agent's dynamics should be affected by some psychological aspects, which we can incorporate, for example, through the agent's level of anxiety

7

described by some dynamic levels, which can constrain the decisions of movement.

Therefore, in our simulations, each agent specifies where it will move according to its stress level. Thus, one or more agents could try to move to the same position simultaneously. In such a case, we will define a collision of intentions between the agents. Hence, the number of collisions C will be a relevant feature in our simulations that we aim to extract from our analysis. The collisions of intentions should help characterize the emergent collective phenomena, unpredictability, and unexpected Brownian-type behavior in specific regimes that occur in the system. When two or more agents want to move to the same cell, we will say that they are in a conflicting movement of pedestrians, which we solve by randomly allowing one of the agents' movement, reducing its stress by one. The remaining agents do not move during the iteration and increase their stress value by one.

We aware that there are many strategies for simulating pedestrian flows, such as those described in terms of force-based models, and in particular limits. We want to note that the agents in our CA are self-propelled, and therefore, the collisions between them are the interactions. In addition, our simulations include nearest and next-to nearest interactions (8 neighboring cells) with the possibility of moving along diagonals. In addition, we could increase the size of the interacting neighborhood of an agent (beyond the eight neighboring cells that it looks to produce a motion intention) and complicate the cell selection process to make it more similar to the discretization of force-based models. Hence, compared to force-based models, our cell size corresponds to the effective length of the repulsive potential, and the range of interaction is at least to the next closest neighbor. Of course, different authors could apply other strategies, but here we tried to balance simplicity in the dynamics with an interpretation of the stress for the agents. Thus, even under our simplifying assumptions, the stress makes a difference in the collective dynamics. Therefore, the interactions in our CA model reflect influential social forces and not necessarily real forces. Also, it suggests that this is a road to chase, and there is much research to do if we want to eventually understand and simulate how crowds move [53, 54].

III. RESULTS

Each individual has a time-varying level of stress that starts at zero and grows or lowers by one step each iteration so that we define threshold values for the separation of the three types

of stress for each individual so that we set threshold values to determine these categories for each individual, namely, U_{I} between mild stress and optimal stress, and U_{II} between optimal stress and anxiety, respectively. Therefore, we define three stress stages, namely, stage I (mild stress), where $0 < \text{stress} \leq U_{\mathrm{I}}$; stage II (optimum stress), where $U_{\mathrm{I}} < \text{stress} \leq U_{\mathrm{II}}$; and stage III (anxiety), where $\text{stress} > U_{\mathrm{II}}$. As an illustration of the results, we start with the upper case of the filled room, and an uniform separation of different thresholds $U_{\mathrm{I}} = d$ and $U_{\mathrm{II}} = 2d$.

We consider an average of 1000 simulations of pedestrians, initially placed at random positions that try to exit the room. We pay attention to the average evacuation time, the percentage of agents on a given stress stage, and the number of collisions of movement intentions.

In Fig. 3 we display how these measures vary with d. For $1/d = 1$, it takes a single clock-tick for an agent to change its stress type, particularly if the agent does not move. We notice that $\langle T \rangle$ changes as we vary d, and reaching a minimum value at around $1/d \approx 10^{-2}$.

Looking at Figs. 3(a)-(b), we note that at $1/d \approx 10^{-3}$ the dynamic is driven by agents that are mainly in mild stress, that is, those that do not try to move until the site of minimal value of FF becomes available. The minimum exit time occurs for a given combination of agents with stress of type I and II, and none of type III. This particular result in our simulation is remarkable since it extends previous results for the individual to the collective dynamics, in which a certain amount of stress can make the system more efficient. As we further increase $1/d$ towards 10^{-1}, the fraction of agents with anxiety increases, which is also reflected in the evacuation time. Finally, when $1/d \approx 1$, the dynamic is driven mainly by agents in the third stress stage, and the evacuation time is the greatest. We want to point out that all the described results are computed for the same value of $\lambda = 3/2$ and agents having an initial stress equal to zero. We have repeated these calculations for agents having random initial stress taken from a uniform distribution between zero stress and $U_{\mathrm{II}} + 1$ (at the start of the 3rd stress stage), and we have obtained very similar results to those shown in this manuscript.

In Fig. 3(c), we show the behavior of the average number collisions of intentions. The probability of losing an attempt to move is always greater than or equal to the probability of winning since many agents may want to move to the same cell, but just one of them finally does it. We expect this behavior to be dominant close to the exit, suggesting that introducing
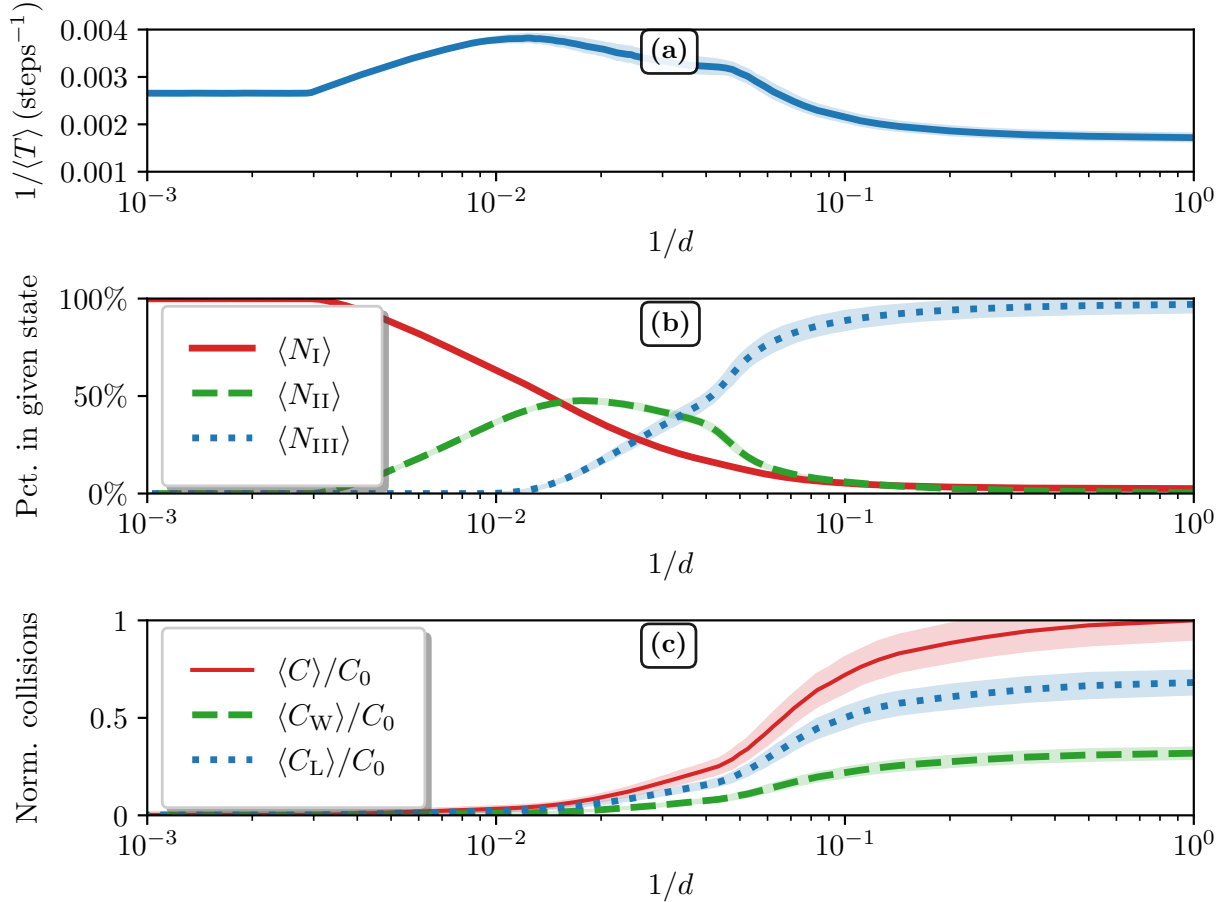
FIG. 3. (color online) These are results for a fully occupied room ($\rho = 1$). In panel (a), with a solid blue line, we show the change of $1/\langle T \rangle$ as d varies. In panel (b), we show the relative fraction of agents in each stress stage. In this panel, with a solid red line, we show the behavior of type or stage I (mild stress); with a dashed green line, we show the behavior of type or stage (optimal stress), and with a dotted blue line, we show the behavior of type or stage III (anxiety). The optimal evacuation time happens when $1/d \sim 10^{-2}$. At this value, we have a combination of agents in the first as second stress stages. The longest evacuation time occurs when most agents are in the third stress stage, denoted by the dotted blue line. In panel (c), with a solid red line, we show the normalized number of total collisions and the average of "won" (green dashed line) and "lost" (blue dotted line) collisions. $C_0 \approx 8 \times 10^6$ normalizes this plot. In all panels, we also present the standard deviations over the 1000 simulations for these measures. Here, $L_x = 18$ and $L_y = 14$.

some strategy to control the agent's stress may reduce the collisions of intention. In our

analysis, introducing a bias for an agent choosing not to move or by putting proper obstacles is expected to lead to a similar result, as by definition, the number of losing collisions should diminish. We wish to explore these in a future manuscript. We want to point out that all these results described in detail do not vary either the initial values of the stress or the value of λ. We have repeated all these calculations for a random distribution of the initial stresses, and we have obtained the same quantitative results.

Now let us examine how the exit time changes as we vary the initial density. In this case, the agents are initially placed randomly in the room to average over an ensemble of initial conditions (and dynamical resolution of conflicts). To observe the dynamics, we select ρ and $1/d$ and plot $T_\rho^{d\to\infty}/\langle T \rangle$, where $T_\rho^{d\to\infty}$ corresponds to the evacuation time for each density ρ when $d \to \infty$ (everyone has mild stress).
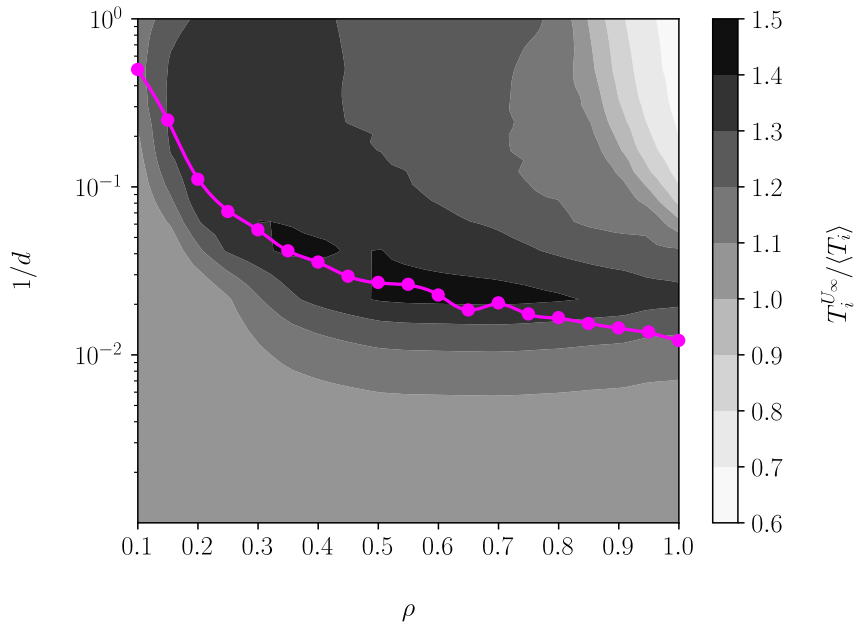

FIG. 4. (color online) Evacuation time as a function of threshold distance d and agent density. We also show the relation of d with ρ (pink line) through the optimal evacuation time curve. Here, in pink points, we show the maximum value for each density.

As expected, Fig. 4 shows that it takes more time to evacuate the room for high densities and small values of d. We also note that for $\rho = 1$, this result is consistent with Fig. 3(a). However, we also note an optimal region of minimal evacuation time (maximal flux), relates to mid densities (for a given mixture of agents with different stress types), which resembles the fundamental diagram of Ref. [55]. That suggests that this is a robust result associated

with a broad class of self-propelled particles. We note that the optimal exit time dependence that relates d with ρ is non-trivial. Therefore, it deserves some study. To understand the transitions, and particularly the dependence of the optimal exit time as we change the densities, we select three different densities ($\rho \in [0.75, 0.5, 0.25]$), which corresponds to $N \in [189, 126, 53]$ agents, respectively. In Fig. 5, we display the average evacuation time, the stress level of the agents, and the average number of collisions.
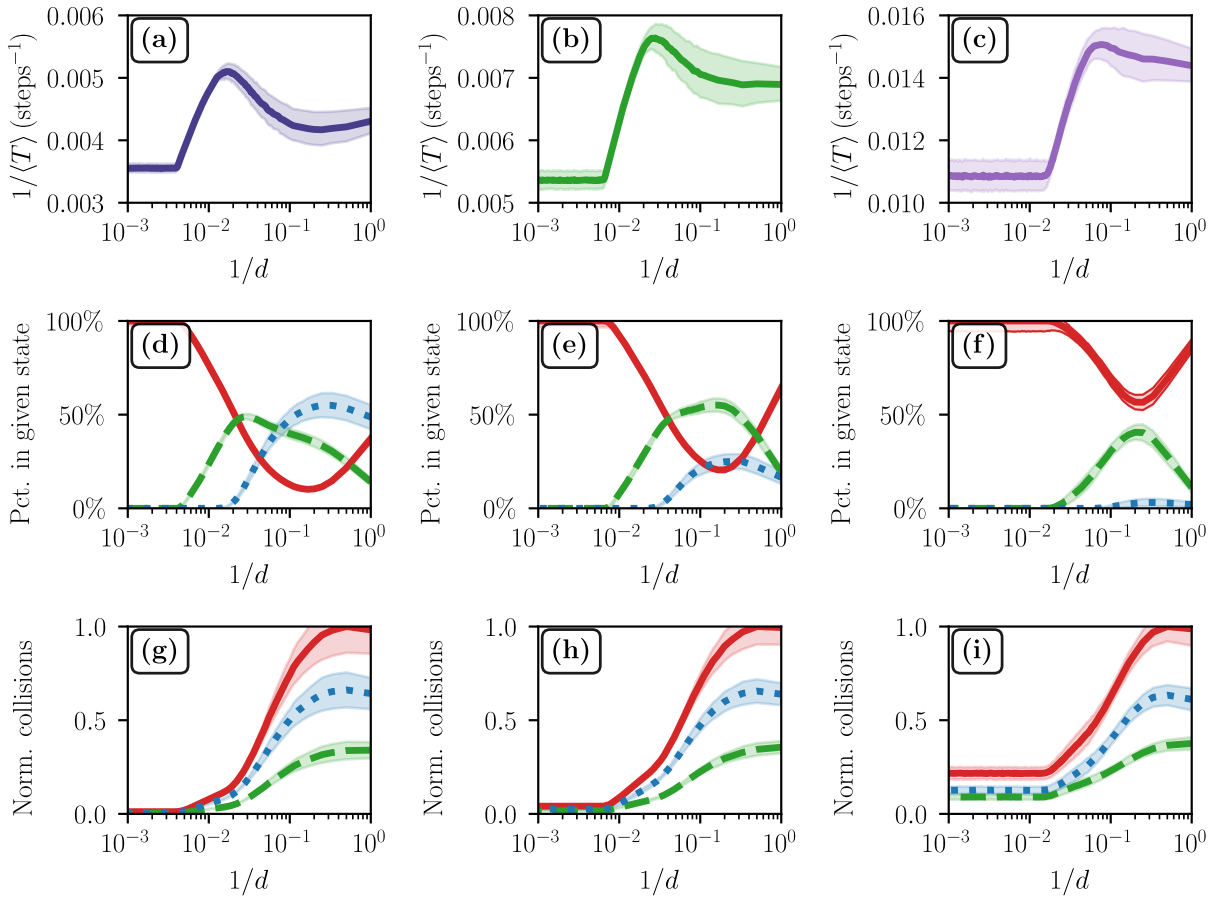

FIG. 5. (color online) In the rows, we show the average evacuation time (top row), average relative number of agents in a given stress stage (middle row), and normalized number of collisions (bottom row); for $\rho = 0.75$ (first column), $\rho = 0.5$ (second column), and $\rho = 0.25$ (third column), respectively. In solid lines (panels (a), (b), and (c)) we show the average evacuation time for each selected density. Panels (g), (h), and (i) are normalized by $C_0 \approx 1.3 \times 10^6$, $C_0 \approx 2.5 \times 10^5$, and $C_0 \approx 2 \times 10^4$, respectively. All the line styles in (d)-(i) follows the convention explained in detail on Fig. 3, and we also present the standard deviations over the 1000 simulations for these measures.

12

We note that the overall evacuation time decreases as we decrease the density, mainly due to two factors: a lower share of agents entering the third stress stage since there is a small number of agents within the room and the collisions of intentions also decrease. The evacuation times for the first two densities (Figs.5(a)-(b)) are similar, while in the diluted case (Fig.5(c)) the evacuation times are remarkably lower. We note that the exit time has an optimal value in all situations, when there is a similar number of agents in the first two stress stages (mild and optimal), and none in the third one (anxiety).

Comparing these plots with those corresponding to the full room ($\rho = 1$, Fig. 3(a)) and higher thresholds ($1/d \in [10^{-3}, 10^{-2}]$), we found that the agents do not move towards the second and third stress stages, so the evacuation times remain constant. However, when the distance between stress thresholds diminishes ($1/d \in [10^{-2}, 10^{-1}]$), the agents can move towards stages of greater stress, diversifying the evacuation paths and lowering the evacuation times. Finally, in the last range ($1/d \in [10^{-1}, 10^{0}]$), as the number of agents spending time in the third stress stage begins to rise, the evacuation time increases, reaching its maximum at this density. For the second selected density ($\rho = 0.75$, Fig. 5(b)), at very high thresholds ($1/d \in [10^{-3}, 10^{-2}]$), we observe the same behavior already described for higher densities. Next, when the distance between thresholds begins to diminish ($1/d \in [10^{-2}, 10^{-1}]$) and recalling that the amount of empty spaces is greater than the previous cases, the agents cannot reach the anxiety stage. However, the standard deviation is much higher since the available choices of movements also increase. Therefore, by selecting previously inaccessible paths, the evacuation time diminishes compared to the higher density situations. For this same threshold range, when the agents are going to stress, stage III starts to decrease, and the evacuation time increases. It also reaches its maximum at this density.

For the third selected density ($\rho = 0.5$, Fig. 5(c)), the dynamic evolves in the same way already observed for higher anxiety thresholds ($1/d \in [10^{-3}, 10^{-2}]$), where the agents do not reach the second and third stress stages, due to the availability of free spaces. Again, the minimal evacuation time occurs for an appropriate combination of agents experiencing mild and optimum stress. We found that the standard deviation raises due to the increased number of accessible paths to the exit. Finally, when the initial density is low, the number of agents reaching the high anxiety level is also low (about 20%).

We have also implemented non-uniform distributions of initial stress. For example, we have taken an initial distribution that resembles a Gaussian profile. For simplicity, we set its

center at zero stress, and its deviation equal to U_I (we only accept positive stress values). We performed evacuation simulations for $\rho \in [1, 0.75, 0.5]$, as shown in Fig. 6. The results are qualitatively similar to those observed above, namely, that the evacuation time reaches an optimal value when we reduce the relative number of agents in the stress state one so that a relatively large number of agents have the flexibility to move to cells that are not necessarily the ones with the lowest floor field in their neighborhood. Of course, there are collective issues, as it becomes difficult to predict the evacuation time solely from the relative number of agents at each of the stress stages. Similarly, the optimal d_{op}, for which the evacuation time is minimal and the minimum of the evacuation time decrease with density. In addition, the minimum value of the evacuation time also decreases with ρ. However, we note from Fig. 6 that the value of d_{op} increases when agents have random initial stress taken from the Gaussian-like distribution, showing that the initial stress level can strongly affect the evacuation time.

Therefore, we have improved the code to display our simulations, and we produced a new version of Fig. 7. In this enhanced version of the code, we now show the tracked agent's stress level, and we display agents' stress levels before and after movement. Now, in the lower-left corner of the tracked agent, we display the agent's stress level when it arrived at the cell, and in the upper right corner is the stress level when the agent leaves the cell.

The notation from the marked agent (specifically in Fig. 7(d), Fig. 7(e) and Fig. 7(f)) shows in the upper part of the cell the number of movements that the specified agent made, and in the lower part in which clock tick the agent moved. Also, the line's color shows what state of stress the agent was in (green if mild stress, yellow if optimal stress, and red if anxiety). The color of the tracked agent shows the level of the stress when the agent arrived in the cell (lower-left corner) and also displays the level of the stress when the agent arrived in the cell (upper-right corner). Finally, we note that all this information is rewritten by the software when an agent revisits a space inside the simulation area (see the agent of Fig. 7(f), between movements 25 and 31). In this interval, the agent revisited these two spaces more than once since it was in anxiety.

We now describe in detail the temporal evolution of a specific agents' stress level. For example, in Fig. 7(d), we track an agent who starts with a low level of stress. In Table I we show in detail each level of stress for all the dynamics of this specific agent.

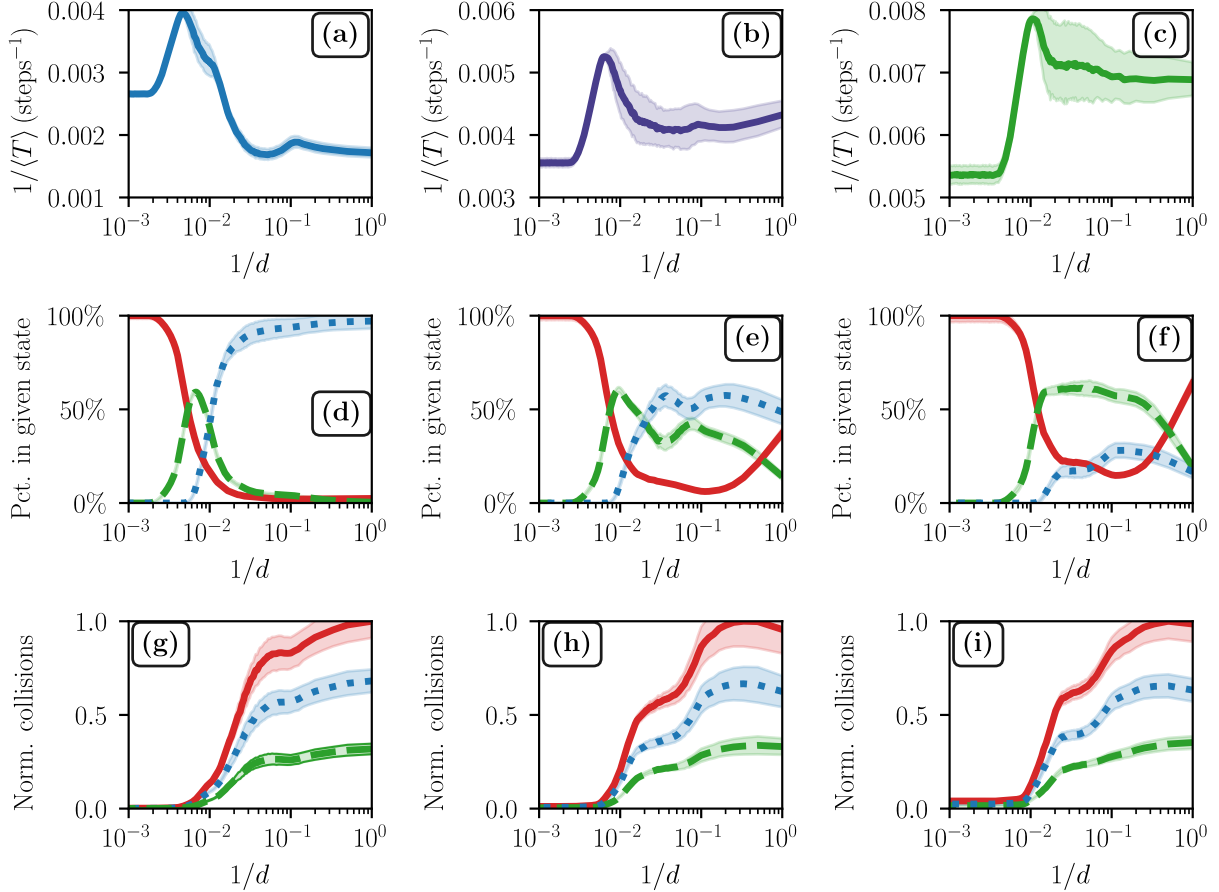With the help of Table I and Fig. 7(d), we can explain in a better way our implementation

FIG. 6. (color online) Results for $1/\langle T \rangle$, percentage in a given stress stage, and normalized collisions for agents having random initial stress taken from a Gaussian distribution. In the rows, we show the average evacuation time (top row), average relative number of agents in a given stress stage (middle row), and normalized number of collisions (bottom row); for $\rho = 1$ (first column), $\rho = 0.75$ (second column), and $\rho = 0.5$ (third column), respectively. Plots (g), (h), and (i) are normalized by $C_0 \approx 8.2 \times 10^6$, $C_0 \approx 1.3 \times 10^6$, and $C_0 \approx 2.5 \times 10^5$, respectively. All the color lines in (d)-(i) follows the convention of Fig. 3, and we also present the standard deviations over the 1000 simulations for these measures. Compared with an uniform initial stress equal to zero (for example, Fig. 5), we observe a different kind of dynamics, that will be analyzed in detail in a future manuscript.

of different stress levels. The agent started in a mild stress situation and kept its position for two iterations. Since $U_I = 5$, when the agent made the first movement was in a mild stress situation. That is why we display the corresponding rectangle in Fig 7(d) with a green rectangle. Therefore, the agent's next movement was made by following the mild stress rules

TABLE I. (color online). Detail of the level of stress for agent 83.

Timestep	Movement?	Stress counter	Stress Level
1	No	1	Mild
2	Yes	0	Mild
3	No	1	Mild
4	No	2	Mild
5	No	3	Mild
6	No	4	Mild
7	No	5	Mild
8	No	6	Optimal
9	Yes	5	Mild
10	No	6	Optimal
11	Yes	5	Mild
12	No	6	Optimal
13	Yes	5	Optimal
14	Yes	4	Mild

are given before, since its stress counter was equal to 1. Afterward, we see that it maintained the position by seven clock ticks, so the optimal stress dominated its following movement rules. Then it managed to make only one movement (the third one), and after that, it remained in its position for five additional clock ticks due to collisions with other agents (losing against them) or inaccessible open cells. The agent could move at the eleventh and thirteenth ticks to exit the simulation in its fifth movement.

The screenshots also highlight two agents' trajectories, namely, agents with Ids 80 and 96 (from left to right panels in Fig. 7(d)), respectively. We choose them because they spend a relevant part of their trajectory in a particular stress level. From Figs. 7(d)-(f) we can conclude that the agents' collisions are essential when the agents approach the door. For example, from Fig. 7(f), we can see that between movements 34 and 35 of the selected agent, seven ticks passed since the door was too crowded and other agents occupy all the tiles. Finally, we can conclude from Fig. 7(f) that the dynamics for the agents, particularly those with high-stress levels, may follow Brownian types of motions. This observation deserves

future study, for it may provide a way to estimate simulation and effective simulation stress level distributions from observations of trajectories of individuals in high-density situations.
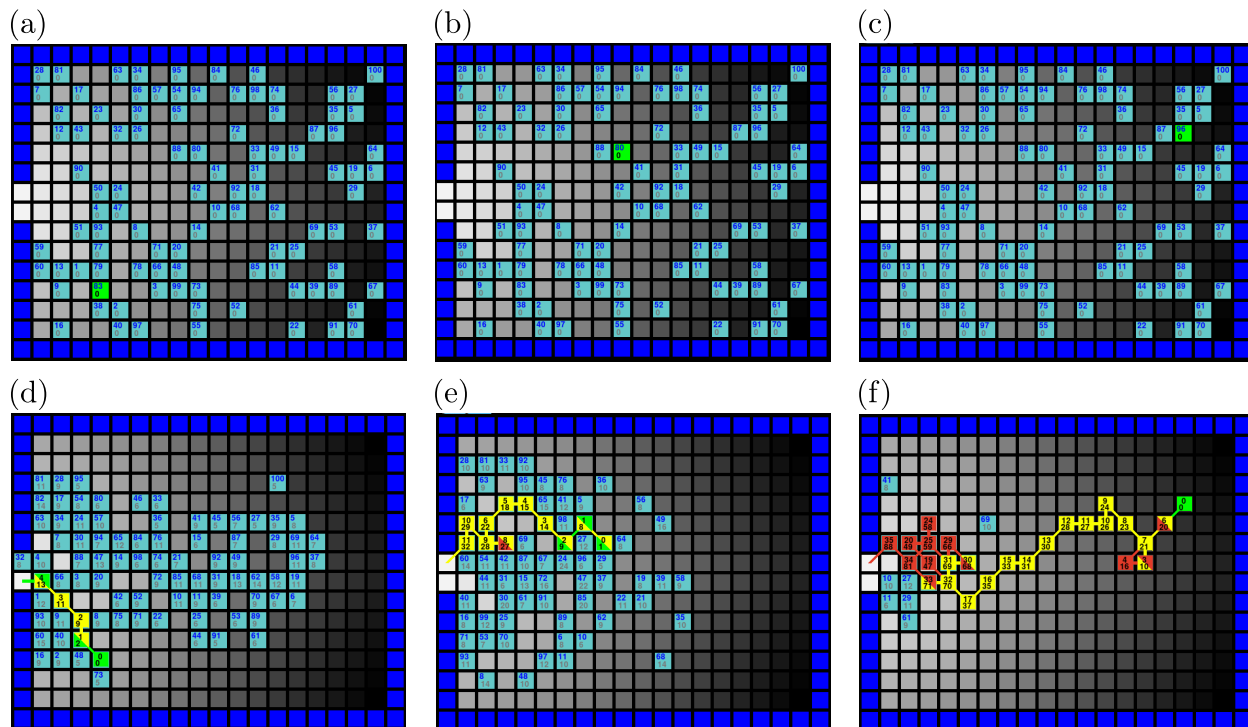

FIG. 7. (color online) In this figure, we show screenshots of three different selected trajectories. In the first row, we plot the initial states of the system, and in the second row, the final state of the system at the time each agent exits, along with the trajectory followed by each agent. We selected these agents to display a combination of mild and optimal stress during the trajectory. The agent's top index of the agent's trajectory numbers the agent's movements, while the bottom index numbers the system's time steps. Also, in the rectangle associated with the tracked agent, we display the agent's stress level, represented by color, in the lower-left side when it arrived at the cell, and on the upper right side, the stress level when the agent leaves the cell. We have used the following color code convention: if the agent is in the first stage (mild stress), we use the green color. If the agent is in the second stage (optimum stress), we use the yellow color; lastly, we use the red color if the agent is in the third stage (anxiety). See Supplemental Material at [URL will be inserted by publisher] for further details on the trajectories.

To produce the above trajectories and overall behavior with density, we expect that the number of collisions should increase rapidly. In Fig. 8 we display the average number of collisions as a function of density for $d = 1$. We note that the number of collisions and

the relative distribution of agent stress become relevant measures that determine the overall dynamics, and one must consider as we consider more realistic pedestrian flows.
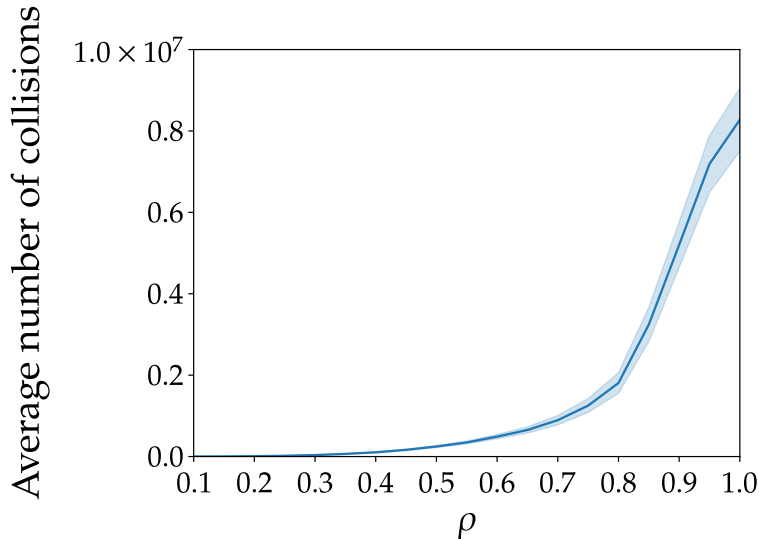

FIG. 8. (color online) The average number of collisions for the complete range of densities and $d = 1$. These simulations were conducted with agents that have zero initial stress. Average number of collisions for the complete range of densities and $d = 1$. These simulations were carried out with agents that have zero initial stress.

IV. CONCLUSIONS

Here we present a model for a group of persons exiting a room without obstacles. In our computer simulations, we implemented a CA using a FF to drive the agents' decisions, which are also affected by their stress level and collisions. Following accepted distinctions of individuals stress, we included three types of agent response depending on the stress type: mild stress, optimum stress, and anxiety. The relative distribution of agents in these three stress stages produce different collective responses; such that for a similar number of agents in the 1st and second stress stages, and none in the 3rd one, we obtain the lowest exit time. This result extends the accepted efficiency from the individual level to the collective behavior. Also, we tracked all the agent's intentions, and they are *collisions of intentions*. Particularly relevant is the notorious difference that the type of stress induces the agent's trajectories when there are enough interactions. This last conclusion is an exciting observation that

deserves more attention in future studies, as it may allow us to relate with the trajectories of individuals in real situations.

Our results with an initially full room show that the dynamics are driven by the relative distribution of agents in the different stress stages, suggesting that this ingredient is an essential aspect that must be considered in evacuation processes. We have assumed that as the agent moves, its anxiety lowers by a fixed amount. In a future study, we plan to challenge this assumption to observe the evacuation time impact.

Although this work extends our recent studies on evacuation times, and particularly as going from 1D to 2D pedestrian flows where there are more movement choices, the results with and without stress are not a direct test of behavior in natural evacuations. Therefore, care should be taken when extrapolating from our findings. However, they provide helpful evidence into the role that different types of stress play in crucial human decision-making, which may help develop more realistic agent-based simulations in the future.

Similarly, it could be of interest to extend this type of analysis to other studies where stress and collisions may become relevant, such as counter flows or multilevel evacuations. The inclusion of psychological stress features into our CA model provides reliable simulations of human evacuation dynamics that can be use to emulate and predict real-world emergency egress from a two-dimensional corridor. We introduce new statistical descriptors for transient states, such as the number of collisions and intentions, to study the collective behavior.

V.   ACKNOWLEDGMENTS

[1] Z. Y. Chen, H. T. Zhang, M. C. Fan, D. Wang, and D. G. Li, Algorithms and experiments on flocking of multiagents in a bounded space, IEEE Trans. Control Syst. Technol. **22**, 1544

(2014).

[2] I. D. Couzin, J. Krause, R. James, G. D. Ruxton, and N. R. Franks, Collective memory and spatial sorting in animal groups, J. Theor. Biol. **218**, 1 (2002).

[3] C. Castellano, S. Fortunato, and V. Loreto, Statistical physics of social dynamics, Rev. Mod. Phys. **81**, 591 (2009).

[4] Z. Zheng, D. Li, and X. Qiu, Experiment and numerical simulation of droplet impact on a sphere particle, International Journal of Research in Engineering and Science **4**, 2320 (2016).

[5] H. Liang, Q. X. Li, B. C. Shi, and Z. H. Chai, Lattice boltzmann simulation of three-dimensional rayleigh-taylor instability, Phys. Rev. E **93**, 033113 (2016).

[6] A. L. Barabasi, The origin of bursts and heavy tails in human dynamics, Nature **435**, 207 (2005).

[7] J. Herbert-Read, Understanding how animal groups achieve coordinated movement, J. Exp. Biol. **219**, 2971 (2016).

[8] P. Westley, A. Berdahl, C. Torney, and D. Biro, Collective movement in ecology: from emerging technologies to conservation and management, Phil. Trans. R. Soc. B **373**, 20170004 (2018).

[9] A. Czirok and T. Vicsek, Collective behavior of interacting self-propelled particles, Physica A **281**, 17 (2000).

[10] J. C. McKinney, A. Tchekhovskoy, and R. D. Blandford, General relativistic magnetohydrodynamic simulations of magnetically choked accretion flows around black holes, MNRAS **423**, 3083 (2012).

[11] H. Y. Wang, X. Q. Yan, and M. Zepf, High-energy monoenergetic proton beams from two stage acceleration with a slow laser pulse, Phys. Rev. ST Accel. Beams **18**, 021302 (2015).

[12] M. Vandenboomgaerde, M. Bonnefille, and P. Gauthier, The Kelvin-Helmholtz instability in national ignition facility hohlraums as a source of gold-gas mixing, Phys. Plasmas **23**, 052704 (2016).

[13] H. Kuang, T. Chen, X. L. Li, and S. M. Lo, A new lattice hydrodynamic model for bidirectional pedestrian flow considering the visual field effect, Nonlinear Dynamics **78**, 1709 (2014).

[14] D. Kahneman, Maps of bounded rationality: Psychology for behavioral economics, Am. Econ. Rev. **93**, 1449 (2003).

[15] G. Gigerenzer, The irrationality paradox, Behav. Brain Sci. **27**, 336 (2004).

[16] U. Hoffrage and T. Reimer, Models of bounded rationality: The approach of fast and frugal

heuristics, Manag. Rev. **15**, 437 (2004).

[17] https://www.youtube.com/watch?v=ehAMLJMiijQ (2020), accessed: 2020-08-26.

[18] https://www.youtube.com/watch?v=tDQw21ntR64 (2020), accessed: 2020-08-26.

[19] D. J. Sumpter, The principles of collective animal behaviour, Phil. Trans. R. Soc. B **361**, 5 (2006).

[20] D. Helbing, I. Farkas, and T. Vicsek, Simulating dynamical features of escape panic, Nature **407**, 487 (2000).

[21] D. Helbing, Traffic and related self-driven many-particle systems, Rev. Mod. Phys. **73**, 1067 (2001).

[22] C. Burstedde, K. Klauck, A. Schadschneider, and J. Zittartz, Simulation of pedestrian dynamics using a two-dimensional cellular automaton, Physica A **295**, 507 (2001).

[23] C. M. Song, Z. H. Qu, N. Blumm, and A. L. Barabasi, Limits of predictability in human mobility, Science **327**, 1018 (2010).

[24] H. S. Niwa, Newtonian dynamical approach to fish schooling, J. Theo. Biol. **181**, 47 (2016).

[25] J. Toner and Y. Tu, Flocks, herds, and schools: a quantitative theory of flocking, Phys. Rev. E **58**, 4828–4858 (1998).

[26] T. Vicsek, A. Czirok, I. Farkas, and D. Helbing, Application of statistical mechanics to collective motion in biology, Physica A **274**, 182–189 (1999).

[27] S. Hubbard, P. Babak, S. Sigurdsson, and K. Magnusson, A model of the formation of fish schools and migrations of fish, Ecol. Model. **174**, 359–374 (2004).

[28] A. Varas, M. D. Cornejo, D. Mainemer, B. A. Toledo, J. Rogan, V. Muñoz, and J. A. Valdivia, Cellular automaton model for evacuation process with obstacles, Physica A **382**, 631 (2007).

[29] M. Ramirez, F. Torres, B. A. Toledo, M. Coello, P. Correa-Burrows, J. Rogan, and J. A. Valdivia, Unpredictability in pedestrian flow: The impact of stochasticity and anxiety in the event of an emergency, Physica A **531**, 121742 (2019).

[30] D. J. Yerkes, The relation of strength of stimulus to rapidity of habit formation, J. Comput. Neurol. Physiol. **18**, 459 (1908).

[31] S. Lupien, F. Maheu, M. Tu, A. Fiocco, and T. Schramek, The effects of stress and stress hormones on human cognition: Implications for the field of brain and cognition, Brain and Cognition **65**, 209 (2007).

[32] J. Adrian, N. Bode, M. Amos, M. Baratchi, M. Beermann, M. Boltes, A. Corbetta, G. Deze-

21

cache, J. Drury, Z. Fu, R. Geraerts, S. Gwynne, G. Hofinger, A. Hunt, T. Kanters, A. Kneidl, K. Konya, G. Köster, M. Küpper, G. Michalareas, F. Neville, E. Ntontis, S. Reicher, E. Ronchi, A. Schadschneider, A. Seyfried, A. Shipman, A. Sieben, M. Spearpoint, G. B. Sullivan, A. Templeton, F. Toschi, Z. Yücel, F. Zanlungo, I. Zuriguel, N. van der Wal, F. van Schadewijk, C. von Krüchten, and N. Wijermans, A glossary for research on human crowd dynamics, Collective Dynamics **4**, 1 (2019).

[33] G. Hofinger, R. Zinke, and L. Kunzer, Human factors in evacuation simulation, planning, and guidance, Transp. Res. Procedia **2**, 603 (2014).

[34] P. Nixon, The human function curve - a paradigm for our times, Act. Nerv. Super. **3**, 130 (1982).

[35] H. Vorst, Evacuation models and disaster psychology, Procedia Engineering **3**, 15 (2010).

[36] M. Moussaid, V. R. Schinazi, M. Kapadia, and T. Thrash, Virtual sensing and virtual reality: How new technologies can boost research on crowd dynamics, Front. Robot. AI **5**, 82 (2018).

[37] M. Moussaid, M. Kapadia, T. Thrash, R. W. Sumner, M. Gross, D. Helbing, and C. Hoelscher, Crowd behaviour during high-stress evacuations in an immersive virtual environment, J. R. Soc. Interface **13**, 20160414 (2016).

[38] H. Vermuyten, J. Beliën, L. D. Boeck, G. Reniers, and T. Wauters, A review of optimisation models for pedestrian evacuation and design problems, Safety Science **87**, 167 (2016).

[39] S. Wolfram, Statistical mechanics of cellular automata, Rev. Mod. Phys. **55**, 601 (1983).

[40] J. von Neumann, *The General and Logical Theory of Automata* (Collected works, 1963).

[41] K. Nagel and M. Schreckenberg, A cellular automaton model for freeway traffic, J. Phys. I France **2**, 2221 (1992).

[42] B. A. Toledo, V. Muñoz, J. Rogan, C. Tenreiro, and J. A. Valdivia, Modeling traffic through a sequence of traffic lights, Phys. Rev. E **70**, 016107 (2004).

[43] A. Varas, M. D. Cornejo, B. A. Toledo, V. Muñoz, J. Rogan, R. Zarama, and J. A. Valdivia, Resonance, criticality and emergence in city traffic through cellular automata, Phys. Rev. E **80**, 056108 (2009).

[44] J. Villalobos, V. Muñoz, J. Rogan, R. Zarama, N. F. Johnson, B. Toledo, and J. A. Valdivia, Regular transport dynamics produce chaotic travel times, Phys. Rev. E **89**, 062922 (2014).

[45] J. Li, S. Y. Fu, H. B. He, H. F. Jia, Y. Z. Li, and Y. Guo, Simulating large-scale pedestrian movement using ca and event driven model: Methodology and case study, Physica A **437**, 304

(2015).

[46] A. Pasculli and C. Audisio, Cellular automata modelling of fluvial evolution: Real and parametric numerical results comparison along river pellice (nw italy), Environ. Model. Assess. **20**, 425 (2015).

[47] M. F. Richele and A. P. F. Atman, Generalized model for solid-on-solid interface growth, Phys. Rev. E **91**, 052407 (2015).

[48] P. Geetha and V. Narayanan, Facial expression analysis for content-based video retrieval, J. Comput. Inf. Sci. Eng. **14**, 041001 (2015).

[49] *Karte - VERKEHR.NRW*, `https://www.verkehr.nrw/` (2020), accessed: 2020-08-10.

[50] J. M. Mateo, Inverted-u shape relationship between cortisol and learning in ground squirrels, Neurobiol. Learn. Mem. **4**, 582 (2008).

[51] P. G. Nixon., The human function curve. with special reference to cardiovascular disorders: part i, The Practitioner **217**, 765 (1976).

[52] P. G. Nixon., The human function curve. with special reference to cardiovascular disorders: part ii, The Practitioner **217**, 935 (1976).

[53] C. Chraibi, U. Kemloh, A. Schadschneider, and A. Seyfried, Force-based models of pedestrian dynamics, Netw. Heterog. Media **6**, 425 (2011).

[54] S. Seer, C. Rudloff, T. Matyus, and N. Brändle, Validating social force based models with comprehensive real world motion data, Transp. Res. Rec. **2**, 724 (2014).

[55] R. D. Kühne and N. H. Gartner, *75 Years of the Fundamental Diagram for Traffic Flow Theory*, Tech. Rep. (Traffic Flow Theory and Characteristics Committee, 2011).